ESA–MOST Dragon Cooperation

中国科技部–欧洲空间局“龙计划”合作

2018 DRAGON 4 MID-TERM RESULTS SYMPOSIUM

2018年“龙计划”四期中期成果国际学术研讨会

**FRI. 21 JUNE 2018**

**DRAGON 4 ID. 32275 PROJECT**

# A NOVEL SPECTRAL FEATURE SET FOR TRACING PROGRESSIVE HOST-PATHOGEN INTERACTION OF YELLOW RUST ON WHEAT IN HYPERSPECTRAL- AND MULTISPECTRAL- IMAGES

YUE SHI, WENJIANG HUANG GIOVANNI LANEVE, STEFANO PIGNATTI, RAFFAELE CASA, QIONG ZHENG, HUIQIN MA, LINYI LIU

19–22 June 2018 | Xi'an, P.R. China

2018年6月19日–22日，中国 西安

01 **Data collection**

02 **Hyperspectral based disease detection**

03 **Satellite based diseases mapping**

04 **Future plan**

01 **Data collection**

02 **Hyperspectral based disease detection**

03 **Satellite based diseases mapping**

04 **Future plan**

# Langfang field work

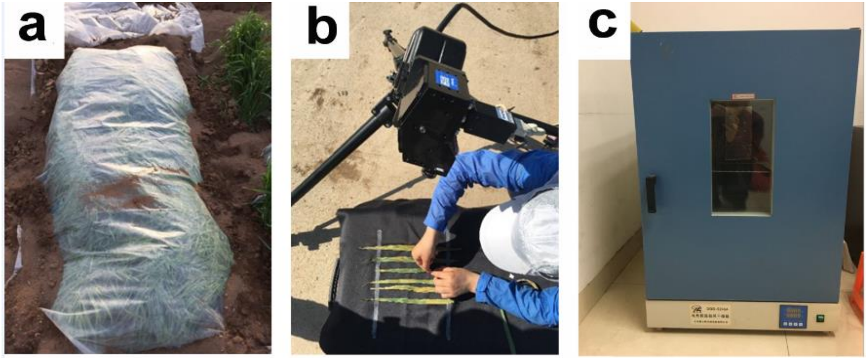


Filed work photo

| Leaf scale | Canopy scale |
|---|---|
| Disease severity | Disease index (DI) |
| Spectral reflectance | Spectral reflectance |
| Imaging spectra | Canopy photos |
| Chlorophyll | Fluorescence |
| Nitrogen balance index | Leaf area index |
| Anthocyanin | |
| Leaf water content | |

Measurements

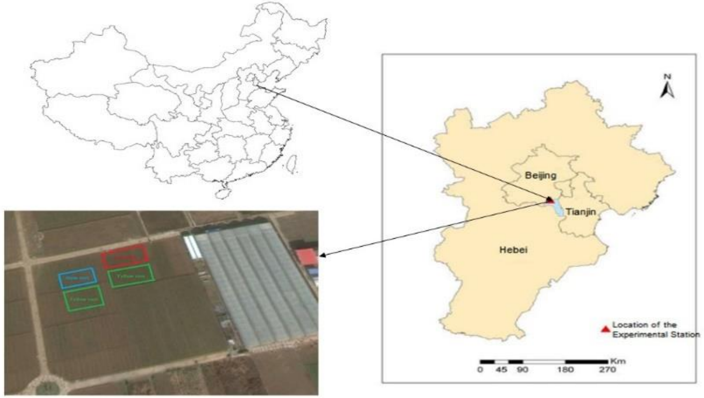


Study site

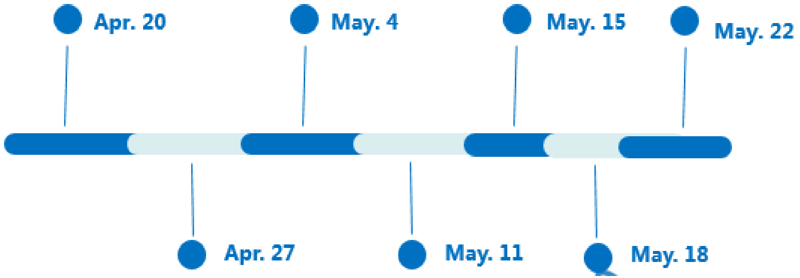


Observations

# Ningqiang investigation

**Experimental site:** Ningqiang county, Hanzhong, Shaanxi province (118°35‘19.51“E, 37°35'51.75“N)

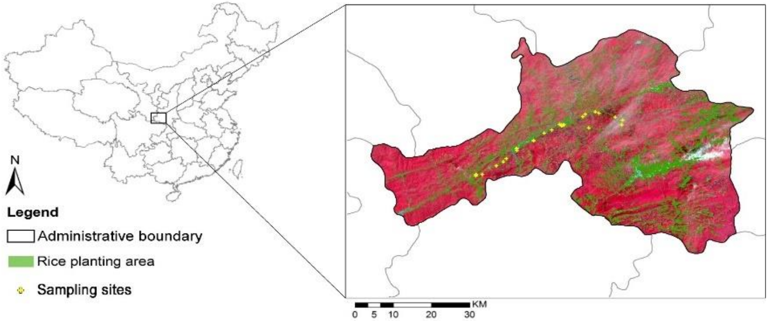


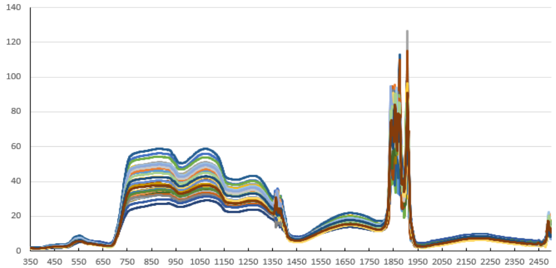


ASD hyperspectral curves

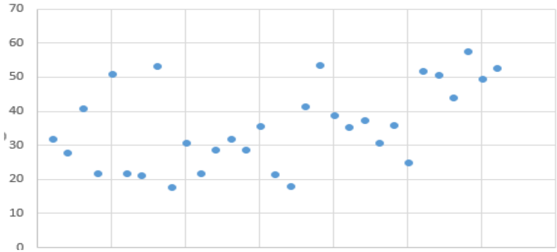


SPAD-values

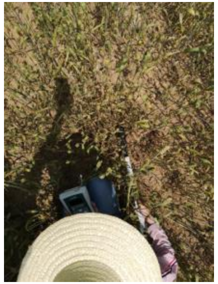

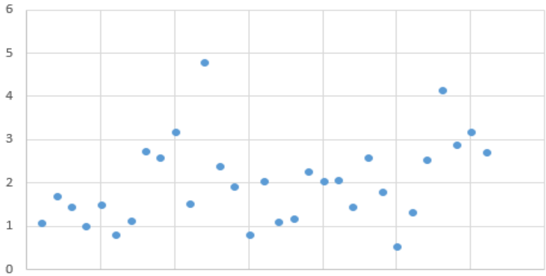


LAI-2200 measurements

01 Data collection

02 **Hyperspectral based disease detection**

03 Satellite based diseases mapping

04 Future plan

# Plant diseases:

Causes:
- Biological infections
- Habitat conditions
- Host

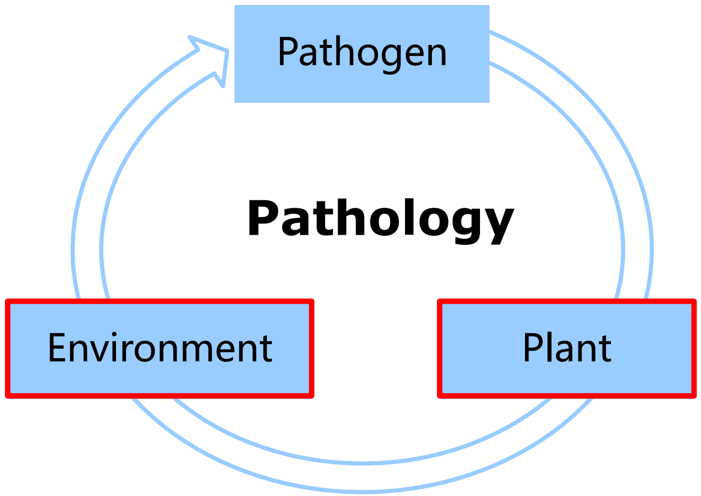


Effects:
- Physiological functions
- Cellular structures
- Morphology

Applications:
- Plant growth --- growth monitoring
- Yield losses --- loss assessment
- Diseases habitat condition --- habitat mapping

# Symptom

Internal symptom

- Discoloration
- Wilting
- Necrosis
- Abnormality
- Rot

External symptom

- Mildew
- Rust
- Powder
- Pus
- Particulate matter




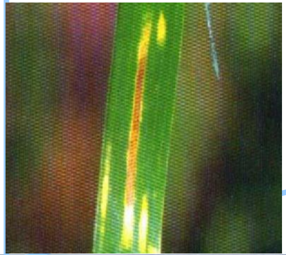
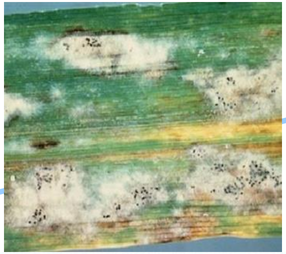


## The progressive development of yellow rust

- The interaction of electromagnetic radiation with plant leaves is governed by their biophysical constituents and response to infestations

- The foliar biophysical variations are critical indicators for tracking the progression of host–pathogen interactions through the different stages

- The development of rust infestation is a complicated process, which is hard to characterize using the preexisting spectral features and methods

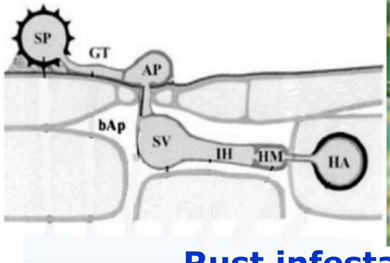


Rust infestation progress

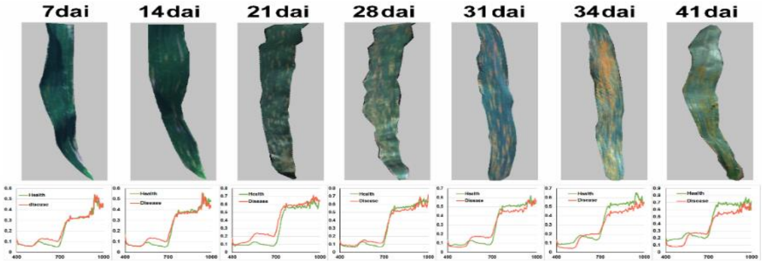


Hyperspectral changes of rust development

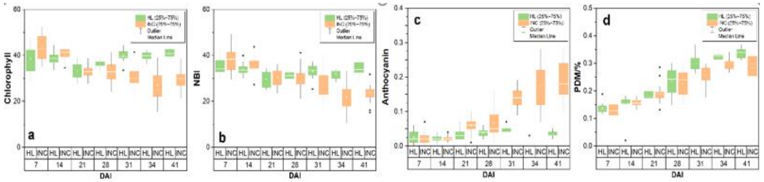


Biophysical changes

## Continuous wavelet transformation (CWT)

A set of wavelet-based rust sensitive features can be characterized by the wavelet coefficients which can be expressed mathematically as:

$$W_f(a,b) = \int_{-\infty}^{+\infty} f(\lambda)\psi_{a,b}(\lambda)d\lambda$$

where f is the original spectrum, n is the number of bands. and ψ is a mother wavelet function:

$$\psi_{a,b}(\lambda) = \frac{1}{\sqrt{a}}\psi\left(\frac{\lambda-b}{a}\right)$$

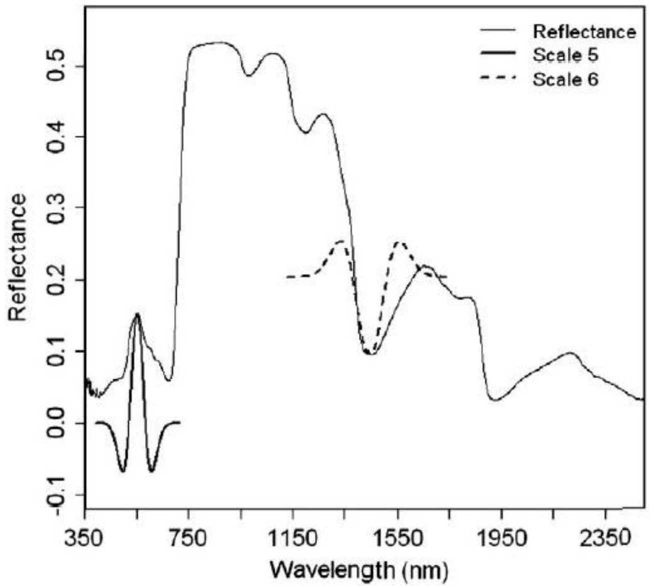

## WRSFs:

The intersection of wavelet features selected from the top 5% of the correlation scalograms from the ASD and Headwall dataset is summarized, a total of 5 feature regions are extracted in blue edge (470 – 485 nm), green peak (520 – 600 nm), and red edge (630 – 760 nm) regions at scales of 2 to 5.

| Wavelet features | Wavelength (nm) | Scale |
|---|---|---|
| **WF01** | 486 | 5 |
| **WF02** | 545 | 2 |
| **WF03** | 571 | 2 |
| **WF04** | 685 | 4 |
| **WF05** | 746 | 4 |

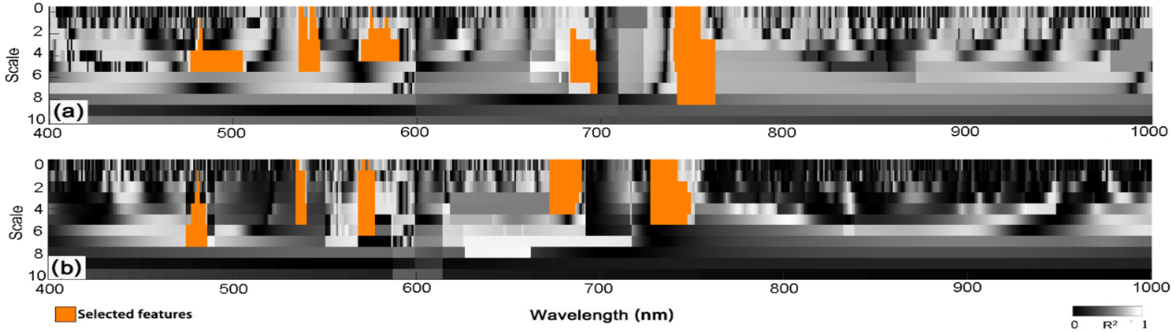

## Correlation analysis

- For the WF01, a significant correlation is observed with the PDM ($R^2$=0.82),
- The biophysical attributes for the WF02 and WF03 are similar, with R2 values of 0.77 and 0.79 for CHL, 0.68 and 0.74 for ANTH,
- For the WF04, a great correlation with NBI and PDM are identified, with R2 value of 0.71 and 0.72
- The correlation between NBI and WF05 is regarded as statistically significant

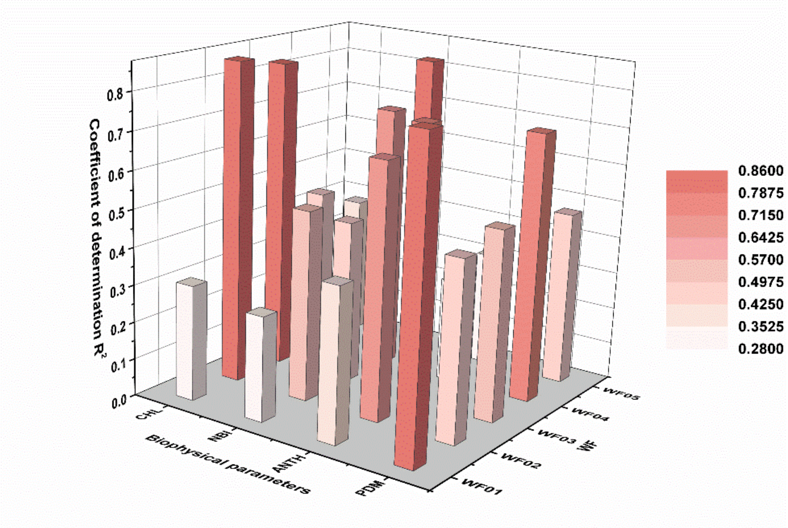

## Retrieving PLS models

For comparison, A total of 9 hyperspectral VIs were selected to compare with the extracted WRSFs for disease detection: modified simple ratio (*MSR*); structural independent pigment index (*SIPI*), normalized pigment chlorophyll index (*NPCI*), antho-cyanin reflectance index (*ARI*), and modified chlorophyll absor-ption reflectance index (*MCARI*) ratio vegetation structure index (*RVSI*); photosynthetic radiation index (*PRI*), physiological reflectance index (*PHRI*); yellow rust index (*YRI*),

| Dai | Feature | PLS-based model equations | R2 | RMSE |
|---|---|---|---|---|
| 7th | WRSFs | DR=0.035-159.45WF01-384.74WF02-60.58WF03 -27.95WF04-65.6WF05 | 0.78 | 0.052 |
| | VIs | DR=-0.054-0.06MSR+0.023PRI+0.136SIPI+0.026NPCI -0.004ARI-0.023YRI | 0.65 | 0.065 |
| 14th | WRSFs | DR=0.16+48.13WF01+220.41WF02-69.34WF03 -103.6WF04-39.68WF05 | 0.81 | 0.045 |
| | VIs | DR=-1.06-0.04MSR+0.56PRI+0.91SIPI+0.2NPCI +0.04ARI-0.49YRI | 0.69 | 0.068 |
| 21st | WRSFs | DR=-0.57-102.29WF01-47.77WF02+25.85WF03 -21.65WF04-8.6WF05 | 0.84 | 0.052 |
| | VIs | DR=-0.937-0.012MSR+0.096PRI+0.38SIPI+0.078NPCI -0.126ARI-0.049YRI | 0.75 | 0.075 |
| 28th | WRSFs | DR=-0.12-23.29WF01+32.98WF02+48.28WF03 +33.42WF04-9.27WF05 | 0.86 | 0.028 |
| | VIs | DR=-0.089-0.018MSR+0.037PRI+0.45SIPI+0.073NPCI -0.015ARI+0.014YRI | 0.73 | 0.037 |
| 31st | WRSFs | DR=-0.07-17.3WF01+82.49WF02-5.02WF03 -44.28WF04-12.39WF05 | 0.91 | 0.019 |
| | VIs | DR=-0.091-0.027MSR+0.125PRI+0.41SIPI+0.102NPCI -0.071ARI-0.085YRI | 0.81 | 0.025 |
| 34th | WRSFs | DR=-0.43-21.4WF01+20.1WF02+50.57WF03 +35.54WF04-14.12WF05 | 0.93 | 0.019 |
| | VIs | DR=-0.125-0.029MSR+0.19PRI+0.646SIPI+0.131NPCI -0.12ARI-0.047YRI | 0.85 | 0.028 |
| 41st | WRSFs | DR=-0.26-18.46WF01-5.26WF02+10.84WF03 -24.4WF04-15.31WF05 | 0.89 | 0.029 |
| | VIs | DRdisease=-0.2-0.037MSR+0.085PRI+0.938SIPI+0.152NPCI -0.24ARI-0.016YRI | 0.82 | 0.031 |

## Yellow rust dynamic monitoring

Before the evident strip-shaped amber uredinium become visible ($7^{th}$ – $21^{st}$ dai), the diseased portions of yellow rust were correctly classified by WRSFs-based SVM with an accuracy range from 84.2% to 95.2%, higher than that of VIs-based SVM with accuracy range of 79.8% to 84.8%. After the first symptoms occurred at $21^{st}$ dai, the classification accuracy *steadily increased* owing to the high spatial resolution obtained by the hyperspectral images. After the 20 day, the classification accuracy was almost consistent to or higher than the visual identification on rust infected leaves.

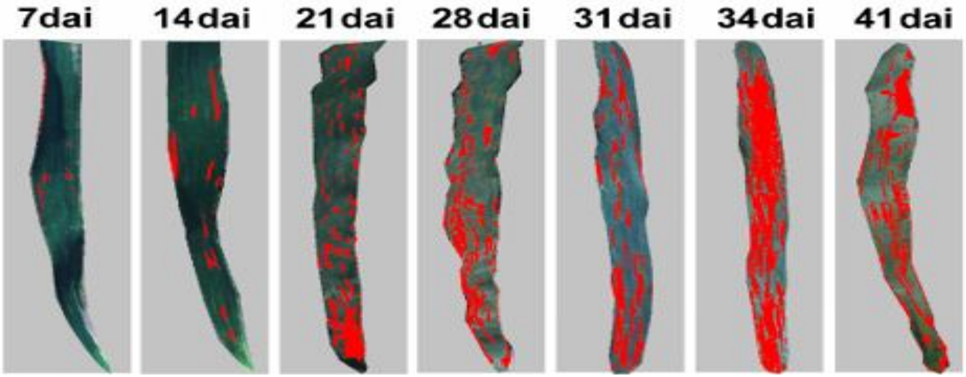


Extraction of rust diseased area produced by WYSFs-based SVM

| Featu re | State | Classification accuracy / % | | | | | | |
|---|---|---|---|---|---|---|---|---|
| | | 7 dai | 14 dai | 21 dai | 28 dai | 31 dai | 34 dai | 41 dai |
| WFs | Health | 88.7 | 92.4 | 97.5 | 99.2 | 98.8 | 96.7 | 98.9 |
| | Diseas e | 84.2 | 90.1 | 95.3 | 97.9 | 100 | 100 | 98.2 |
| VIs | Health | 73.5 | 81.2 | 88.6 | 95.4 | 96.9 | 95.2 | 96.1 |
| | Diseas e | 80.5 | 84.8 | 79.8 | 92.7 | 98.2 | 98.4 | 98.5 |

01 Data collection

02 Hyperspectral based disease detection

03 Satellite based diseases mapping

04 Future plan

# Sentinel-2 data

| Spectral Band | | Centre Wavelength (nm) | Spatial Resolution (nm) |
|---|---|---|---|
| B1 | Coastal aerosol | 443 | 60 |
| B2 | Blue (B) | 490 | 10 |
| B3 | Green (G) [1] | 560 | 10 |
| B4 | Red (R) [1] | 665 | 10 |
| B5 | Red-edge 1 (Re1) [1] | 705 | 20 |
| B6 | Red-edge 2 (Re2) [1] | 740 | 20 |
| B7 | Red-edge 3 (Re3) [1] | 783 | 20 |
| B8 | Near infrared (NIR) [1] | 842 | 10 |
| B8a | Near infrared narrow (NIRn) [1] | 865 | 20 |
| B9 | Water vapor | 945 | 60 |
| B10 | Shortwave infrared/Cirrus | 1380 | 60 |
| B11 | Shortwave infrared 1(SWIR1) | 1910 | 20 |
| B12 | Shortwave infrared 2(SWIR2) | 2190 | 20 |

March 28, 2018

May 12, 2018

# Feature selection

- Pathologically, the progressive development between the various disease infestations are different, although these infestations may lead to similar external symptoms.
- Considering the potential pathological impact of disease infestations mentioned above, six vegetation indices (VIs) that related to plant growth, vegetation coverage, and radiant absorption of pigments were selected.

*Normalized Two-Stage Vegetation Indices*：

$$VI_{two-stage} = \frac{VI_{30October} - VI_{21August}}{VI_{30October} + VI_{21August}}$$

| Definition | Sensitive to |
|---|---|
| **Normalized difference vegetation index, NDVI** | Green biomass |
| **Soil-adjusted vegetation index, SAVI** | Canopy structure |
| **Triangular vegetation index, TVI** | Radiant absorption of chlorophyll |
| **Re-normalize difference vegetation index, RDVI** | Vegetation coverage |
| **Modified Simple Ratio, MSR** | Leaf area, Biomass |
| **Structural Independent Pigment Index, SIPI** | Pigments content |

- For healthy rice, the normalized two-stage vegetation indices revealed greater differences with the rice infested with disease compared to corresponding single-date VIs from the images on 30 October
- For the diseased rice, the responses of the newly proposed normalized two-stage vegetation indices were strongly associated with the individual pathological progress of different diseases.

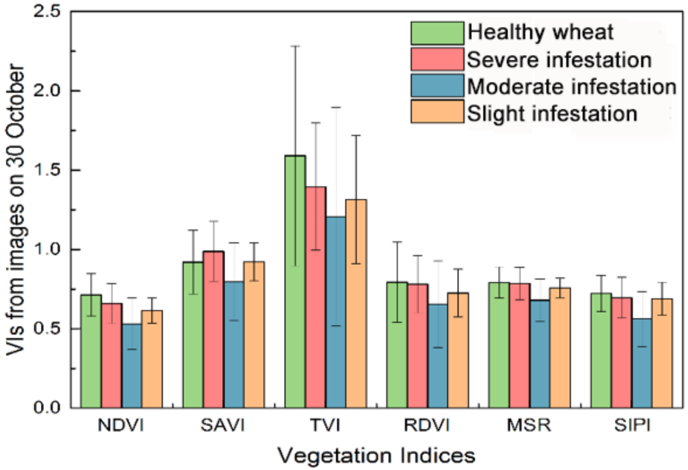


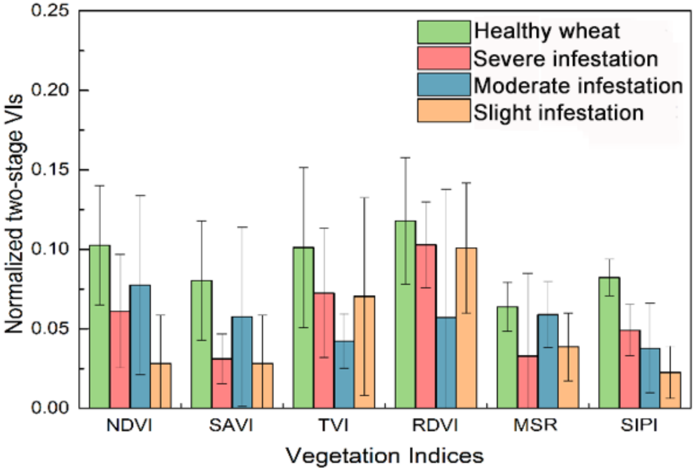

## Support vector machine:

- In the SVM classification frame, the optimal margin would be outputted by *maximizes the distance* between the *hyperplane* and the *nearest points of both classes*, and then achieves the best prediction for unlabeled points

- The separation decided by a kernel function reflects *the merits of the components and structure of input feature space*, because the kernel function comprises an implicit mapping of samples in order to characterizing the input feature space.

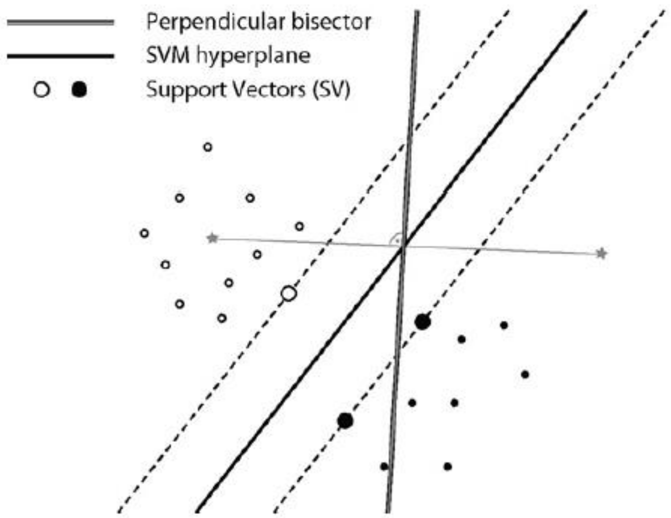

| Predicted Class | Healthy Rice | Rice Dwarf | Rice Blast | Glume Blight | User's Accuracy (%) | Overall Accuracy (%) | Kappa Coefficient |
|---|---|---|---|---|---|---|---|
| **Normalized two-stage VIs** | | | | | | | |
| **Healthy rice** | 54 | 0 | 6 | 2 | 87.1 | 75.62 | 0.47 |
| **Rice dwarf** | 4 | 60 | 5 | 9 | 76.92 | | |
| **Rice blast** | 11 | 4 | 48 | 5 | 70.59 | | |
| **Glume blight** | 5 | 8 | 2 | 27 | 64.29 | | |
| **Producer's accuracy (%)** | 72.97 | 83.33 | 78.69 | 62.79 | | | |
| **single-date VIs** | | | | | | | |
| **Healthy rice** | 47 | 3 | 8 | 4 | 75.81 | 61.67 | 0.27 |
| **Rice dwarf** | 8 | 48 | 5 | 17 | 61.54 | | |
| **Rice blast** | 16 | 6 | 39 | 7 | 57.35 | | |
| **Glume blight** | 7 | 11 | 4 | 20 | 47.62 | | |
| **Producer's accuracy (%)** | 60.26 | 70.59 | 69.64 | 41.67 | | | |

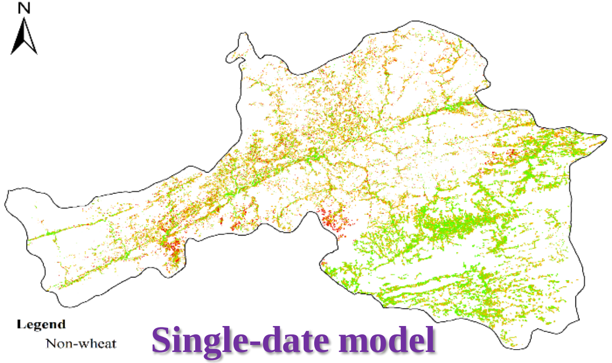


Single-date model

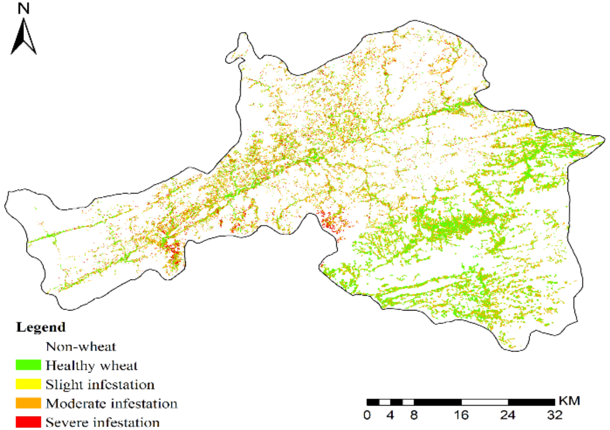


Normalized two-stage model

01 Data collection

02 Hyperspectral based disease detection

03 Satellite based diseases mapping

04 Future plan

Rust detection and classification

1

## Evaluations

Evaluate the robustness of the proposed spectral features of yellow rust by using the historical hyper-spectral data

2

## Calibration

Optimize the parameters of the developed classifiers of rust infestation, and generalize their applications

3

## Novel descriptor

Develop a novel vegetation index based on the broad bands of new launched satellites for direct detection of rust infestation

4

## Regional applications

Utiize our achievements on the new launched satellites for guiding the crop management.